JACS Au
AN OPEN ACCESS JOURNAL OF THE AMERICAN CHEMICAL SOCIETY

pubs.acs.org/jacsau

Letter

Improving the Stability and Efficiency of Perovskite Solar Cells by a Bidentate Anilinium Salt

Lucas Scalon, Rodrigo Szostak, Francineide L. Araújo, Karla F. Adriani, Julian F. R. V. Silveira, Willian X. C. Oliveira, Juarez L. F. Da Silva, Caio C. Oliveira,* and Ana Flávia Nogueira*

Cite This: *JACS Au* 2022, 2, 1306−1312

Read Online

ACCESS | Metrics & More | Article Recommendations | Supporting Information

ABSTRACT: We report improvement in the perovskite solar cell efficiency and stability after passivation with an organic molecule decorated with two anilinium cations. We compare this salt with its neutral analog and found that the change in the electron density distribution upon protonation and the presence of the halide anion are key to explaining the better passivation ability of the salt. In addition, we show that the counteranion has a significant impact on the performance of the device.

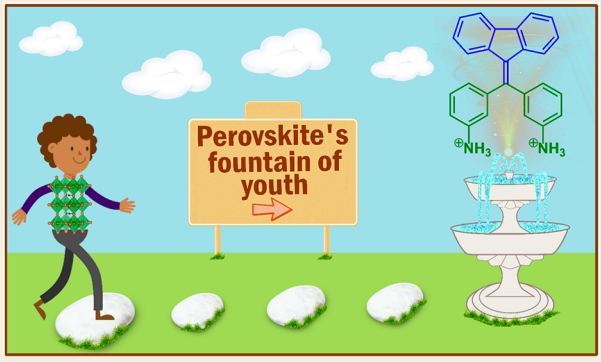

KEYWORDS: *defect passivation, stable perovskite solar cells, aggregation-induced luminogen, DFT calculation, rational synthesis*

Hybrid organic−inorganic perovskites (HOIP) are promising materials for fabricating efficient solar cells because of the high optical absorption coefficient, direct bandgap, long lifetime, diffusion length, and mobility of the charge carriers.[1] HOIP adopts a cubic-like structure (Figure 1) with the general formula ABX_3, where A is a monovalent organic/inorganic cation, e.g., formamidinium (FA^+), methylammonium (MA^+), and cesium (Cs^+), B is a divalent metal (e.g., Pb^{2+} and Sn^{2+}), and X a halide anion (I^-, Br^-, Cl^-). One of the outstanding properties of these materials is their defect tolerant ability.[2] This is because, in the bulk, most of the low-formation energy defects form shallow levels near the band edges,[3,4] becoming populated because of thermal energy. Therefore, those intrinsic defects are not critical to impact the solar cell performance. Nevertheless, the solution-processed methods used to fabricate perovskite films result in dangling bonds on the surface and in a polycrystalline material with grain boundaries (GB) over the film. These two types of defects are responsible for decreasing the device's efficiency: From one side, the dangling bonds increase the density of trap states on the surface,[5] in addition to work as a nonradiative recombination center for the photogenerated charge carriers, thereby reducing the open-circuit voltage (V_{OC}) of the perovskite solar cell (PSC).[6−8] On the other hand, GB can facilitate the moisture and oxygen permeation,[9] act as nonradiative recombination centers,[10−12] and cause hysteresis behavior of the current density *vs.* voltage (J−V) curve.[13] In this context, it is clear that the surface is a critical point of PSC performance and stability. For this reason, interface engineering strategies are an important key. An approach to obtaining the desired passivating effect lies in the post-treatment of the film using conjugated organic molecules.[14−16] Playing with the Lewis acid and base chemistry of the functional groups, it is possible to passivate positively and negatively charged defects.[2,17−21]

Also, there is an explicit concern about the PSC production under sustainable and cost-effective conditions.[22−25] An approach to reach these goals is the replacement of the toxic halogenated solvents used as antisolvent to prepare perovskite film. Among the strategies, we highlight the development of gas quenching methods,[26−29] which triggers the perovskite crystallization by blowing an inert gas on the film. Combining this innovative method with postpassivation strategies, it is possible to obtain efficient, stable, and more sustainable devices.

Herein, we report the synthesis of a newly designed organic molecule, the 3,3′-((9H-fluoren-9-ylidene)methylene)dibenzenaminium (**FM-NH_3X**, Figure 1), decorated with two anilinium cations, designed to passivate $FAPbI_3$-based PSCs produced by the gas quenching method. When compared to the neutral molecule analog, the salt presents a superior

Received: March 4, 2022
Revised: April 28, 2022
Accepted: April 29, 2022
Published: May 4, 2022

https://doi.org/10.1021/jacsau.2c00151
JACS Au 2022, 2, 1306−1312

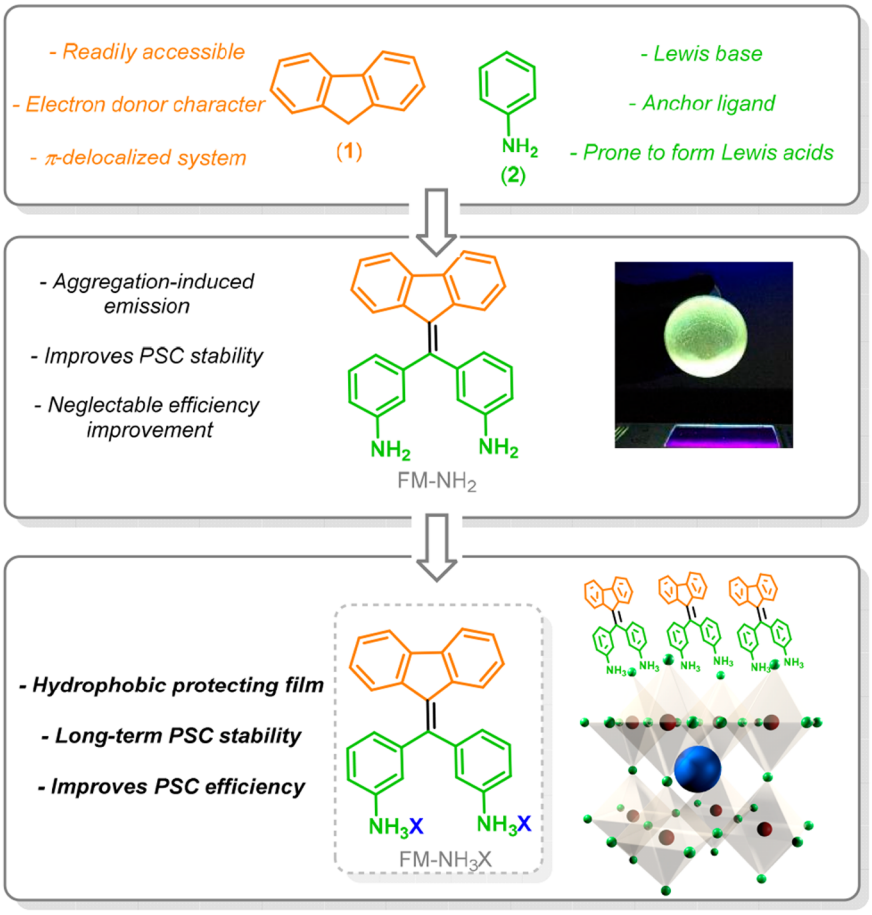

Figure 1. Schematic illustration of the molecules designed and their interaction with an ABX_3 perovskite (in the scheme, A, B, and C cations are the blue, red, and green spheres, respectively).

passivation effect, leading to efficiencies of ∼19% and stability for more than 90 days.

To design our passivating molecules (Figure 1), we were inspired by two commonly used structural moieties: fluorene (**1**) and aniline (**2**). The former is known for its planar conjugated backbone and electron donation properties.[30] The latter is a Lewis base, able to interact with Lewis acid defects on the perovskite. We coupled the aniline with the fluorene using the Corey−Fuchs reaction,[31] yielding the **FM-NH$_2$** (Figure 1). This molecule presents clear characteristics of aggregation-induced emission (AIE) luminogen: a feature that can be explored in the passivation of PSC. Further, the protonation of **FM-NH$_2$** with hydrogen halides (HX, where X is Cl, Br, or I) yielded anilinium salts (**FM-NH$_3$X**). Sections 1 and 3 in the Supporting Information show the detailed experimental procedure and the full characterization, respectively, of the molecules synthesized. Note that the amino group in our molecules is attached directly to the conjugated backbone. As a result, the electron-donating and hydrogen-bonding (HB) ability of the −NH$_2$ group is weakened compared to alkylamine molecules because of the resonance effect.[32] A weaker HB was reported to benefit the defect passivation of perovskite films.[32] In addition, annilinium-based salts were found to improve the physical contact between the perovskite and the hole transport material (HTM), in the case of *nip*-type PSC.[33] In both neutral and protonated molecules, the formation of HB with iodide is expected to heal ionic vacancies in the film.[34,35]

We investigated the efficiency of the passivation effect of **FM-NH$_2$** in the $FAPbI_3$-based films. To this end, we assembled PSCs with an architecture FTO/SnO_2/$Cs_{0.05}FA_{0.95}Pb(I_{0.95}Br_{0.05})_3$/*modification*/Spiro-OMeTAD/Au. Scanning electron microscopy (SEM) images reveal the formation of an amorphous film of **FM-NH$_2$** coating the perovskite (Figure S14). Despite this, we observed that the perovskite passivation with **FM-NH$_2$** in a concentration range from 4 to 16 mM does not cause any impact on the solar cell performance (Figure S15a). However, the changes in the contact angle of the film denote a tendency of the neutral molecule to decrease moisture permeation (Figure S15b). Such improvement can be explained in terms of the orientation of the molecules: From our Density Functional Theory (DFT) calculations, the fluorene moiety on **FM-NH$_2$** points outward to the surface, creating hydrophobic protection, whereas the polar **−NH$_2$** groups interact with perovskite directly (Section 6 in the Supporting Information).

With the aim of improving the efficiency while keeping similar hydrophobic protection, we protonated the neutral molecule with HX, yielding a class of **FM-NH$_3$X** salts. These salts were used to passivate the perovskite film in the same way as the neutral molecule. The prepared devices showed reduced hysteresis (Table S9); hence, to simplify the discussion, we present only the results of the backward scan measurements (Figure 2a, b). In general, the post passivation with the salts increases the efficiency of the PSCs, as shown in Figure 2a. A table summarizing the device parameters obtained after 10

https://doi.org/10.1021/jacsau.2c00151
JACS Au 2022, 2, 1306−1312

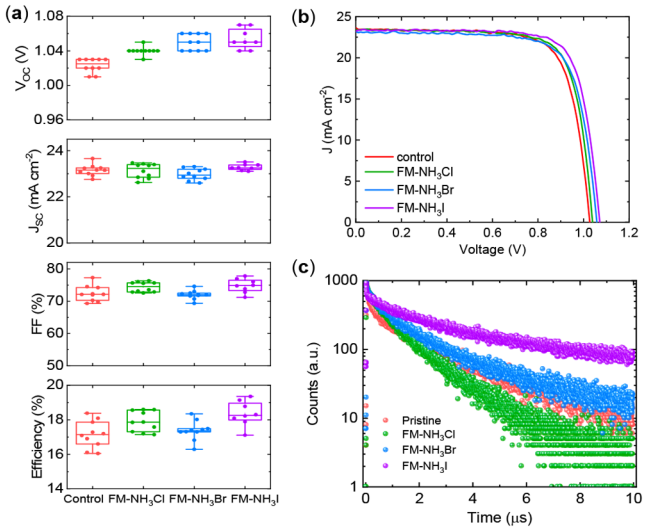

Figure 2. (a) Statistics of the device performance with the post-treatment with the **FM-NH$_3$X** salts. (b) $J-V$ curve of the champion device efficiency. (c) Time-resolved photoluminescence (TRPL) decay curves of the perovskite film modified with **FM-NH$_3$X** onto a glass substrate.

days of stabilization is shown in Section 9 in the Supporting Information. The main improvements were observed in the V_{OC}, which we attribute to healing of the surface defects. Also, the fill factor (FF) increases slightly (about 2%, on average), which can be assigned to a smoother interface with the HTM. In particular, we note that the V_{OC} improvements are dependent on the halide nature, with the highest average values found for bromine- and iodide-based salts. Such a dependence is also evident in the time-resolved photoluminescence (TRPL) measurements: from the control to **FM-NH$_3$Br** and **FM-NH$_3$I**, the TRPL increases from 591 to 601 and 1125.4 ms, respectively. Those results indicate that the halide anion impacts the defect passivation.[36] In the literature, bromide and iodide have been shown to cause band bending at the interface[37] and the passivation of halide vacancies,[38] respectively, which can explain the V_{OC} and charge carrier lifetime improvements obtained in our work. As a result of the passivation, the highest average efficiency (18.36%) was achieved for the salt with iodide, followed by chloride (17.91%), and bromide (17.37%). The average efficiency of the control device was equal to 17.15%. Our champion device, obtained after **FM-NH$_3$I** passivation, shows V_{OC}, FF, short-circuiting current (J_{SC}), and efficiency equals 1.07 V, 23.51 mA cm^{-2}, 77.82%, and 19.35% (Figure 2b), respectively.

To understand how the salts modify the surface, we characterized the films by X-ray diffraction (XRD) and Fourier transform infrared (FTIR) spectroscopy (Figures S16 and S17). From XRD, we cannot find any significant difference between the control and passivated films. On the other hand, FTIR shows the emergence of a band between 2800 and 3000 cm^{-1}, which can be ascribed to the aromatic C−H stretching of the salt. Because the X-ray can penetrate deeply into the film, our results revealed that the modifications affect only the surface, with no (or undetectable) impact on the bulk of the perovskite.

Further, we used X-ray photoemission spectroscopy (XPS) to probe the surface modifications and investigate the interaction between the perovskite and the passivating molecules. From the C 1s high-resolution spectra of the pristine film, we can see an intense peak at ∼288.5 eV corresponding to the oxidation of the organic component of the perovskite structure (FA molecules) by oxygen and/or moisture (Figure S18a).[15] Interestingly, after the passivation with the **FM-NH$_3$X**, the intensity of this peak is highly

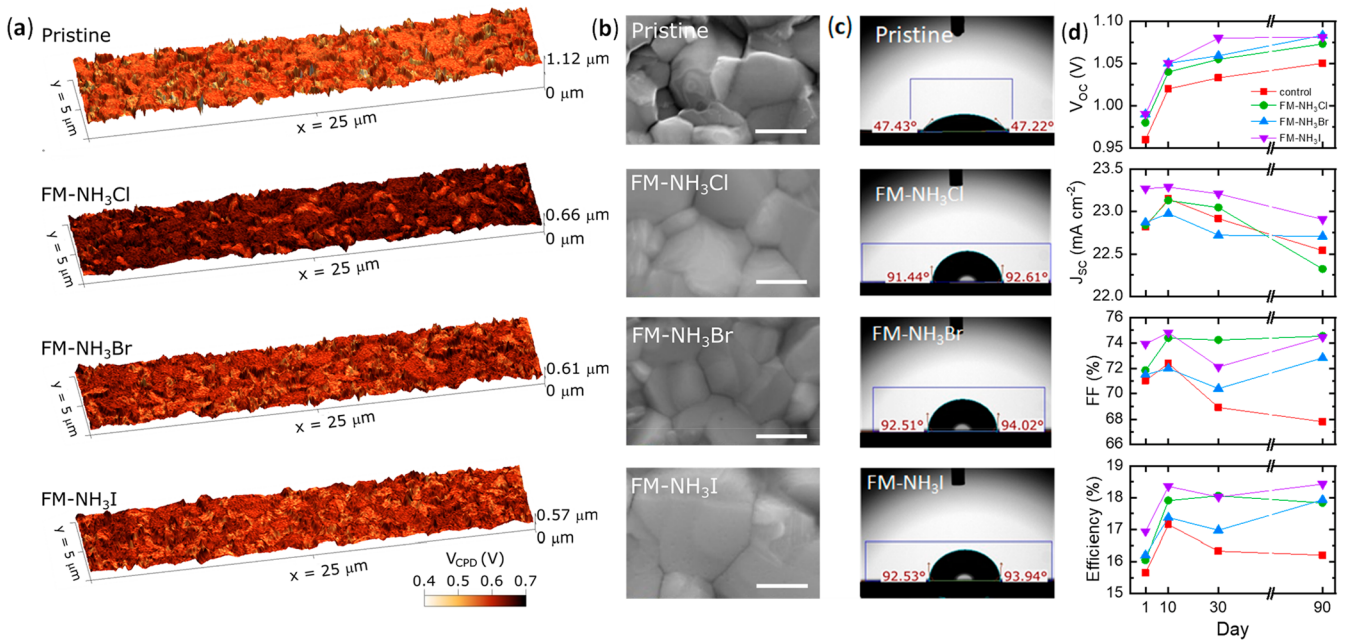

Figure 3. (a) AFM and KPFM merged images, (b) SEM, and (c) contact angle measurements of the perovskite film treated with **FM-NH$_3$X** (where X = Cl, Br, I). (d) Evolution of the solar cell parameters upon aging. The devices were stored in an N_2-filled box, with humidity <30%. The V_{CPD} in panel a was obtained as an average between the 50 000 pixels of the image. The scale bar in panel b is 1 μm.

https://doi.org/10.1021/jacsau.2c00151
JACS Au 2022, 2, 1306−1312

suppressed, indicating that the organic salts help to decrease the film degradation.

Also, XPS can give insights into toward the formation/passivation of iodide vacancies (V_I). This type of defect is very detrimental to PSC's long-term efficiency because it triggers the degradation of the perovskite in several ways. For instance, the formation of superoxide species ($O_2 + e^- \rightarrow O_2^-$) is facilitated by V_I, which causes irreversible perovskite degradation.[39] In addition, iodide vacancies facilitate moisture permeation by solvating the Pb species.[40] To study V_I by XPS, we need to look at the Pb 4f high-resolution spectra. Once V_I is present, the electron left by the released I atom ($2I^- \rightarrow I_2(g) + 2e^-$) is mainly located at the vacant site,[41] allowing it to reduce the uncoordinated Pb^{2+} ion to yield metallic lead ($Pb^{2+} + 2e^- \rightarrow Pb^0$). The formation of Pb^0 results in a small shoulder close to the main peaks of Pb $4f^{7/2}$ and Pb $4f^{5/2}$ in the XPS spectra.[42] In our case, it was possible to identify those shoulders only in the case of the pristine and **FM-NH$_2$**-treated films at an energy equal to 137.8 and 142.6 eV (Figure S18c).[43,44] However, in the cause of neutral molecule, the area of the Pb^0-related peaks decreased by 32% regarding the pristine film, suggesting a passivating effect conferred by **FM-NH$_2$** due to both the lone pairs on the nitrogen atom and the electron cloud over the molecule. The main changes are seen upon salt treatment, in which the intensity of Pb^0 signals is highly suppressed, meaning that these molecules retard the formation of metallic lead. Because it is one of the products generated by V_I formation the absence of the signal corresponding to Pb^0 suggests the passivation of iodide vacancy.[45] Note that only the salts can effectively prevent the formation of Pb^0. This can be explained by the presence of the halide counteranion and by the nature of the molecular orbital distribution, which changes significantly upon protonation (Figure S11). Both of these effects allow the salt to have an electron-donation behavior, which can lead to the passivation of electron acceptor-type of defects, *e.g.*, V_I.[42,46] Further evidence of this passivating effect is seen by the shift of Pb 4f peaks toward lower energy, suggesting an increased electron density over the Pb^{2+} conferred by the salt molecules. The mitigation of V_I is one of the reasons behind the improved V_{OC} of the salt-treated device.

The surface passivation is also expected to impact the morphology of the perovskite film. Using atomic force microscopy (AFM) measurements (Figure 3a), we verified that the average roughness (R_a) changes from 67 nm for the control to 52, 58, and 55 nm for **FM-NH$_3$X**, with X = **Cl$^-$**, **Br$^-$**, and **I$^-$**, respectively, suggesting a smoother and more uniform surface. Further, SEM measurements revealed that the grain size of our perovskite films is larger than 1 μm, even for the control sample, which is a reflection of their good quality (Figure 3b). In addition, SEM shows a less defined grain boundary upon passivation, which can be attributed to the filling of the intergrain voids by the molecules because of its soft molecular backbone. In principle, a smooth surface could benefit the contact between the perovskite layer and the HTM (in our case, Spiro-OMeTAD).[47,48]

Concomitantly with the AFM measurement, we performed Kelvin probe force microscopy (KFPM) to map the surface potential. Briefly, in KPFM, we measured the contact potential difference (V_{CPD}) between the sample and the AFM tip. This quantity can be correlated with the Fermi energy (E_F) of the sample and the tip as follows: $V_{CPD} \propto E_{F,\,sample} - E_{F,\,tip}$. Hence, it is possible to probe how the E_F of the surface is affected by the interaction with the molecules. A more detailed discussion about the KPFM can be found in Section 13 in the Supporting Information. The KPFM maps (Figure 3a) show that the average V_{CPD} changes from 520 mV for the pristine film to 447, 488, and 553 mV for **FM-NH$_3$X**, with X = Cl, Br, and I, respectively, revealing the impact of the counteranion in the modulation of the surface E_F. At a first approximation, we can conclude that the E_F of the films modified with **FM-NH$_3$Cl** and **FM-NH$_3$Br** are shifted upward compared to the pristine film. On the other hand, the salt with iodide presented a downward shift. As suggested by Chen et al.,[49] a deep E_F can allow a better energy match with the highest occupied molecular orbital (HOMO) of the Spiro-OMeTAD, facilitating the charge extraction and decreasing the bimolecular charge carrier recombination at the interface. This result is in line with the TRPL measurements and the device's performance, which point out an enhancement in the average lifetime and V_{OC}, respectively, upon the treatment with **FM-NH$_3$I**. Combining the results, we can conclude that the better passivation effect observed for the salt with iodide is due to a combined effect of V_I passivation, improved electron density over the fluorene moiety, and decreased bimolecular recombination at the surface.

Despite finding that the I-based salt resulted in the best performance, other works in the literature showed that Br^--[37] or Cl^--based[50] salts confer a superior passivation effect. The conflicting results reported by different groups reveal that it is quite hard to predict the exact role of the counteranion in the overall device efficiency as well as in the electronic and photophysical properties of the perovskite. This is because the formation of a passivating or 2D layer onto the film depends[51] on the perovskite composition, the purity of the precursors, the method of thin-film preparation, and the device architecture. Because all these parameters influence the defect concentration and surface energy of the perovskite, the role of the counteranion is not a predictable parameter, and variations are thus expected.

Further, we verified the effect of the salts in retarding the degradation of the PSC by tracking the device's efficiency for 90 days (Figure 3d). The postpassivation, especially for **FM-NH$_3$I**, was effective at preventing device degradation, keeping average efficiencies near 18%. This effect is assigned to the decreased moisture permeation into the film. Also, the grain boundary and ionic vacancy passivation,[52] as well as the suppressed oxidation of the organic components in the perovskite film (see XPS results), could help decrease film degradation. The increased hydrophobicity conferred by the **FM-NH$_3$X** salts can be seen by the contact angle measurements, which increase from 47 to 92° upon the salt treatment (Figure 3c). It is worth noting that, at the same concentration (*i.e.*, 8 mM), the neutral molecule, **FM-NH$_2$**, has a smaller effect on the contact angle when compared to the protonated molecules (Figure S15b and Figure 3c). These observations suggest that the cationic molecules interact strongly with each other when compared to the neutral analog, which is in line with a recent study on the interaction of organic cations by π-stacking interactions.[53] Such a conclusion is also supported by the fact that the electron density is higher on the fluorene moiety in the salt when compared to the **FM-NH$_2$**, benefiting the intermolecular $\pi-\pi$ interactions (Figure S5a).

Finally, to understand in more detail how the protonated and neutral molecules interact with the perovskite surface, we created models varying (i) the particular orientation of the NHx groups in the molecules, (ii) the relative orientation of

https://doi.org/10.1021/jacsau.2c00151
JACS Au 2022, 2, 1306−1312

the molecules on top of the perovskite slab, and (iii) the termination of the perovskite surface. The details of the calculation and the results obtained were shown in Section 6 in the Supporting Information. We studied eight models: four containing the neutral covering a 2 × 2 × 3 $FAPbI_3$ neutral slab where the FAI salt was removed from the surface, allowing the molecules to interact with Pb and I atoms (Figure S12), and the other four containing the protonated molecules covering a 2 × 2 × 3 $FAPbI_3$ negatively charged slab where only the FA was removed, allowing **FM-NH_3** to effectively replace the FA molecules (Figure S13). In each group of four, the models were differentiated by the rotation of the aniline/anilinium group regarding the fluorene moiety, as well as the distribution of the molecules on the surface. This was done to ensure proper sampling of the different possible configurations and to evaluate possible energetic preferences.

With the calculations, we determined the average energy associated with the interaction, adsorption, and distortion, E_i, E_a, and E_d, respectively, measured as meV/Å^2. We found that these values amount to -15.43, −12.61, and 2.81 for $FAPbI_3$+**FM-NH_2**, and −110.73, −91.86, and 18.88 for $FAPbI_3$+**FM-NH_3**. These results are consistent and show that the protonated molecules effectively establish an ionic bond with the surface, whereas the neutral molecule has only weak van der Waals (vdW) interactions. Thus, the fact that the interaction of the first is seven times stronger is coherent. This number would probably be higher if not for the increased distortion associated with the interaction of the protonated molecule with the perovskite. Using an alkylammonium chain, instead of the amine connected directly with the aromatic ring, for instance, should decrease this distortion, since there will be more degrees of freedom for the molecule to adopt a configuration with minimized impact on the organization of the lead octahedra on the surface. However, a deeper discussion on this topic goes beyond the scope of this article.

To further understand how molecule orientation and position affect total energy, we evaluated the dispersion energy associated with the different components of the system, as well as the dispersion energy directly associated with the interaction between perovskite and molecules. To do so, we calculate the optimized geometry structure of the different isomers of **FM-NH_2** and **FM-NH_3** (Section 5 in the Supporting Information). Those isomers differ from the relative position of the amine group, yielding three analogs: up−up, up−down, and down−down (see Figure S7). We found that the down−down configuration had slightly stronger dispersion energy (0.5 eV). Consequently, it possesses a stronger vdW contribution associated with the molecules stacking on the perovskite surface. This stacking was more compact than the up−up stacking, for instance, as it brought the fluorene moieties closer. This better packing of the molecule in the down−down configuration benefits $\pi-\pi$ stacking interactions, which supports the formation of a hydrophobic protective film that decreases moisture permeation into the perovskite. Additionally, the dispersion associated with the interaction between molecules and surface was shown to be stronger in the $FAPbI_3$+**FM-NH_3** systems (2.37 eV on average, against 1.53 eV for $FAPbI_3$+**FM-NH_2** systems), which shows that the stronger interaction observed is a combination of Coulombic and vdW interactions.

In summary, we prepare $FAPbI_3$ perovskite by the gas quenching method using a bidentate anilinium salt as a post-treatment of the film. With this approach, we obtained efficiencies up to 19% stable for more than 90 days. We demonstrated that the use of a salt derived from an AIE-luminogen, when compared to its neutral counterpart, was effective in passivating iodide vacancies on the surface of the film, in addition to creating a better protective barrier against moisture permeation. We found that the outperformance of the salt is related to the localization of the electron wave function on the fluorene moiety, which is beneficial to the passivation of iodide vacancies along with improving molecule−molecule interaction. We also showed that the counteranion of the salt substantially affects the E_F of the surface. Hence, the design of new passivating agents should also include the selection of the best counteranion, which will depend on several parameters highlighting the environment of the amino group in the molecule, and the composition of the perovskite used. In future works, we intend to focus on the optimization of the perovskite layer, aiming to improve the efficiency of the device beyond the 19% obtained here.

■ ASSOCIATED CONTENT

Supporting Information

The Supporting Information is available free of charge at https://pubs.acs.org/doi/10.1021/jacsau.2c00151.

Experimental details and characterization of the molecules synthesized, computational methods, scanning electron microscopy, infrared spectroscopy, X-ray diffraction, X-ray photoelectron spectroscopy, statistics of the perovskite solar cells modified with $FM-NH_2$, and comment about Kelvin probe force microscopy measurements (PDF)

■ AUTHOR INFORMATION

Corresponding Authors

Caio C. Oliveira − *Institute of Chemistry, University of Campinas, Campinas, São Paulo 13083-970, Brazil;* orcid.org/0000-0002-2277-8003; Email: caio.oliveira@unicamp.br

Ana Flávia Nogueira − *Institute of Chemistry, University of Campinas, Campinas, São Paulo 13083-970, Brazil;* orcid.org/0000-0002-0838-7962; Email: anafla@unicamp.br

Authors

Lucas Scalon − *Institute of Chemistry, University of Campinas, Campinas, São Paulo 13083-970, Brazil;* orcid.org/0000-0002-3222-6560

Rodrigo Szostak − *Institute of Chemistry, University of Campinas, Campinas, São Paulo 13083-970, Brazil*

Francineide L. Araújo − *Institute of Chemistry, University of Campinas, Campinas, São Paulo 13083-970, Brazil*

Karla F. Adriani − *São Carlos Institute of Chemistry, University of São Paulo, São Carlos, São Paulo 13560-970, Brazil*

Julian F. R. V. Silveira − *São Carlos Institute of Chemistry, University of São Paulo, São Carlos, São Paulo 13560-970, Brazil*

Willian X. C. Oliveira − *Department of Chemistry, Federal University of Minas Gerais, Belo Horizonte, Minas Gerais 31270-901, Brazil*

Juarez L. F. Da Silva − *São Carlos Institute of Chemistry, University of São Paulo, São Carlos, São Paulo 13560-970, Brazil;* orcid.org/0000-0003-0645-8760

https://doi.org/10.1021/jacsau.2c00151
JACS Au 2022, 2, 1306−1312

Complete contact information is available at:
https://pubs.acs.org/10.1021/jacsau.2c00151

Author Contributions

L.S. synthesized and characterized the materials, designed the experiments, and wrote the original draft. R.S. optimize the method for the preparation of perovskite films, assembled and characterized the devices. F.L.A. helped with device characterization. K.F.A., J.F.R.V.S., and J.L.F.S. performed the theoretical calculations. W.X.C.O. performed the single-crystal XRD characterization. L.S., C.C.O., and A.F.N. conceived the idea and conceptualized the work. C.C.O. and A.F.N. supervised the project. All the authors revised the paper.

Notes

The authors declare no competing financial interest.

■ ACKNOWLEDGMENTS

The authors gratefully acknowledge support from FAPESP (São Paulo Research Foundation, Grant Numbers 2017/11631-2 and 2018/21401-7), Shell and the strategic importance of the support given by ANP (Brazil's National Oil, Natural Gas and Biofuels Agency) through the R&D levy regulation. C.C.O. acknowledges FAPESP (grants 2018/01669-5 and 2014/25770-6). We also thank the National Council for Scientific and Technological Development (CNPq) and the Center for Innovation on New Energies (CINE). L.S. acknowledges FAPESP (grants 2019/08257-7 and 2020/04406-5). R.S. acknowledges FAPESP (grant 2017/12582-5). K.F.A., J.F.R.V.S., and J.L.F.S. gratefully acknowledge support from FAPESP (grants 2017/11631-2 and 2018/21401-7). K.F.A. acknowledges FAPESP (grant 2018/11152-0). F.L.A. acknowledges FAPESP (grant 2020/14451-8).

■ REFERENCES

(1) Kim, J. Y.; Lee, J. W.; Jung, H. S.; Shin, H.; Park, N. G. High-Efficiency Perovskite Solar Cells. *Chem. Rev.* **2020**, *120* (15), 7867−7918.
(2) Dunfield, S. P.; Bliss, L.; Zhang, F.; Luther, J. M.; Zhu, K.; Hest, M. F. A. M.; Reese, M. O.; Berry, J. J. From Defects to Degradation: A Mechanistic Understanding of Degradation in Perovskite Solar Cell Devices and Modules. *Adv. Energy Mater.* **2020**, *10* (26), 1904054.
(3) Yin, W. J.; Shi, T.; Yan, Y. Unusual Defect Physics in CH3NH3PbI3 Perovskite Solar Cell Absorber. *Appl. Phys. Lett.* **2014**, *104* (6), 063903.
(4) Chen, B.; Rudd, P. N.; Yang, S.; Yuan, Y.; Huang, J. Imperfections and Their Passivation in Halide Perovskite Solar Cells. *Chem. Soc. Rev.* **2019**, *48* (14), 3842−3867.
(5) Ni, Z.; Xu, S.; Huang, J. Response to Comment on "Resolving Spatial and Energetic Distributions of Trap States in Metal Halide Perovskite Solar Cells. *Science* **2021**, *371*, 1352−1358.
(6) Wang, F.; Bai, S.; Tress, W.; Hagfeldt, A.; Gao, F. Defects Engineering for High-Performance Perovskite Solar Cells. *NPJ Flexible Electronics* **2018**, *2*, 22.
(7) Wu, S.; Zhang, J.; Li, Z.; Liu, D.; Qin, M.; Cheung, S. H.; Lu, X.; Lei, D.; So, S. K.; Zhu, Z.; Jen, A. K. Y. Modulation of Defects and Interfaces through Alkylammonium Interlayer for Efficient Inverted Perovskite Solar Cells. *Joule* **2020**, *4* (6), 1248−1262.
(8) Jiang, Q.; Zhao, Y.; Zhang, X.; Yang, X.; Chen, Y.; Chu, Z.; Ye, Q.; Li, X.; Yin, Z.; You, J. Surface Passivation of Perovskite Film for Efficient Solar Cells. *Nat. Photonics* **2019**, *13* (July), 460−466.
(9) Yun, J. S.; Kim, J.; Young, T.; Patterson, R. J.; Kim, D.; Seidel, J.; Lim, S.; Green, M. A.; Huang, S.; Ho-baillie, A. *Humidity-Induced Degradation via Grain Boundaries of HC (NH 2) 2 PbI 3 Planar Perovskite Solar Cells* **2018**, *28* (11), 1705363.
(10) Yin, W.-J.; Yang, J.-H.; Kang, J.; Yan, Y.; Wei, S.-H. Halide Perovskite Materials for Solar Cells: A Theoretical Review. *J. Mater. Chem. A* **2015**, *3*, 8926−8942.
(11) de Quilettes, D. W.; Vorpahl, S. M.; Stranks, S. D.; Nagaoka, H.; Eperon, G. E.; Ziffer, M. E.; Snaith, H. J.; Ginger, D. S. Impact of Microstructure on Local Carrier Lifetime in Perovskite Solar Cells. *Science (80-.)* **2015**, *348* (6235), 683−686.
(12) An, Q.; Paulus, F.; Becker-Koch, D.; Cho, C.; Sun, Q.; Weu, A.; Bitton, S.; Tessler, N.; Vaynzof, Y. Small Grains as Recombination Hot Spots in Perovskite Solar Cells Small Grains as Recombination Hot Spots in Perovskite Solar Cells. *Matter* **2021**, *4*, 1683−1701.
(13) Shao, Y.; Fang, Y.; Li, T.; Wang, Q.; Dong, Q.; Deng, Y.; Yuan, Y.; Wei, H.; Wang, M.; Gruverman, A.; Shield, J.; Huang, J. Grain Boundary Dominated Ion Migration in Polycrystalline Organic-Inorganic Halide Perovskite Films. *Energy Environ. Sci.* **2016**, *9* (5), 1752−1759.
(14) Jiang, Q.; Ni, Z.; Xu, G.; Lin, Y.; Rudd, P. N.; Xue, R.; Li, Y.; Li, Y.; Gao, Y.; Huang, J. Interfacial Molecular Doping of Metal Halide Perovskites for Highly Efficient Solar Cells. *Adv. Mater.* **2020**, *32*, 2001581.
(15) Zhuang, J.; Mao, P.; Luan, Y.; Yi, X.; Tu, Z.; Zhang, Y.; Yi, Y.; Wei, Y.; Chen, N.; Lin, T.; Wang, F.; Li, C.; Wang, J. Interfacial Passivation for Perovskite Solar Cells: The Effects of the Functional Group in Phenethylammonium Iodide. *ACS Energy Lett.* **2019**, *4* (12), 2913−2921.
(16) Gharibzadeh, S.; Fassl, P.; Hossain, I. M.; Rohrbeck, P.; Frericks, M.; Schmidt, M.; Duong, T.; Khan, M. R.; Abzieher, T.; Nejand, B. A.; et al. Two Birds with One Stone: Dual Grain-Boundary and Interface Passivation Enables >22% Efficient Inverted Methylammonium-Free Perovskite Solar Cells. *Energy Environ. Sci.* **2021**, *14* (11), 5875−5893.
(17) Lee, S.; Park, J. H.; Lee, B. R.; Jung, E. D.; Yu, J. C.; Di Nuzzo, D.; Friend, R. H.; Song, M. H. Amine-Based Passivating Materials for Enhanced Optical Properties and Performance of Organic−Inorganic Perovskites in Light-Emitting Diodes. *J. Phys. Chem. Lett.* **2017**, *8* (8), 1784−1792.
(18) Li, Z.; Jo, B. H.; Hwang, S. J.; Kim, T. H.; Somasundaram, S.; Kamaraj, E.; Bang, J.; Ahn, T. K.; Park, S.; Park, H. J. Bifacial Passivation of Organic Hole Transport Interlayer for NiO x -Based P-i-n Perovskite Solar Cells. *Adv. Sci.* **2019**, *6* (6), 1802163.
(19) Zheng, X.; Chen, B.; Dai, J.; Fang, Y.; Bai, Y.; Lin, Y.; Wei, H.; Zeng, X. C.; Huang, J. Defect Passivation in Hybrid Perovskite Solar Cells Using Quaternary Ammonium Halide Anions and Cations. *Nat. Energy* **2017**, *2* (7), 1−9.
(20) Wang, N.; Zhao, K.; Ding, T.; Liu, W.; Ahmed, A. S.; Wang, Z.; Tian, M.; Sun, X. W.; Zhang, Q. Improving Interfacial Charge Recombination in Planar Heterojunction Perovskite Photovoltaics with Small Molecule as Electron Transport Layer. *Adv. Energy Mater.* **2017**, *7* (18), 1700522.
(21) Said, A. A.; Xie, J.; Zhang, Q. Recent Progress in Organic Electron Transport Materials in Inverted Perovskite Solar Cells. *Small* **2019**, *15* (27), 1900854.
(22) Chang, N. L.; Zheng, J.; Wu, Y.; Shen, H.; Qi, F.; Catchpole, K.; Ho-Baillie, A.; Egan, R. J. A Bottom-up Cost Analysis of Silicon−Perovskite Tandem Photovoltaics. *Prog. Photovoltaics Res. Appl.* **2021**, *29* (3), 401−413.
(23) Zhao, B. X.; Yao, C.; Gu, K.; Liu, T.; Xia, Y.; Loo, Y.-L. A Hole-Transport Material That Also Passivates Perovskite Surface Defects for Solar Cells with Improved Efficiency and Stability. *Energy Environ. Sci.* **2020**, *13* (11), 4334−4343.
(24) Bauer, M.; Zhu, H.; Baumeler, T.; Liu, Y.; Eickemeyer, F. T.; Lorenz, C.; Mena-Osteritz, E.; Hertel, D.; Olthof, S.; Zakeeruddin, S. M.; Meerholz, K.; Grätzel, M.; Bäuerle, P. Cyclopentadiene-Based Hole-Transport Material for Cost-Reduced Stabilized Perovskite Solar Cells with Power Conversion Efficiencies Over 23%. *Adv. Energy Mater.* **2021**, *11*, 2003953.
(25) Wang, Y.; Liao, Q.; Chen, J.; Huang, W.; Zhuang, X.; Tang, Y.; Li, B.; Yao, X.; Feng, X.; Zhang, X.; Su, M.; He, Z.; Marks, T. J.; Facchetti, A.; Guo, X. Teaching an Old Anchoring Group New

Tricks: Enabling Low-Cost, Eco-Friendly Hole-Transporting Materials for Efficient and Stable Perovskite Solar Cells. *J. Am. Chem. Soc.* **2020**, *142* (39), 16632−16643.
(26) Taylor, A. D.; Sun, Q.; Goetz, K. P.; An, Q.; Schramm, T.; Hofstetter, Y.; Litterst, M.; Paulus, F.; Vaynzof, Y. A General Approach to High-Efficiency Perovskite Solar Cells by Any Antisolvent. *Nat. Commun.* **2021**, *12* (1), 1878.
(27) Szostak, R.; Sanchez, S.; Marchezi, P. E.; Marques, A. S.; Silva, J. C.; Holanda, M. S.; Hagfeldt, A.; Tolentino, H. C. N.; Nogueira, A. F. Revealing the Perovskite Film Formation Using the Gas Quenching Method by In Situ GIWAXS: Morphology, Properties, and Device Performance. *Adv. Funct. Mater.* **2021**, *31* (4), 2007473.
(28) Zhang, M.; Bing, J.; Cho, Y.; Li, Y.; Zheng, J.; Lau, C. F. J.; Green, M. A.; Huang, S.; Ho-Baillie, A. W. Y. Synergistic Effect of Potassium and Iodine from Potassium Triiodide Complex Additive on Gas-Quenched Perovskite Solar Cells. *Nano Energy* **2019**, *63* (April), 103853.
(29) Tang, S.; Bing, J.; Zheng, J.; Tang, J.; Li, Y.; Mayyas, M.; Cho, Y.; Jones, T. W.; Yang, T. C.-J.; Yuan, L.; Tebyetekerwa, M.; Nguyen, H. T.; Nielsen, M. P.; Ekins-Daukes, N. J.; Kalantar-Zadeh, K.; Wilson, G. J.; McKenzie, D. R.; Huang, S.; Ho-Baillie, A. W. Y. Complementary Bulk and Surface Passivations for Highly Efficient Perovskite Solar Cells by Gas Quenching. *Cell Reports Phys. Sci.* **2021**, *2* (8), 100511.
(30) Scalon, L.; Leithold Neto, A.; Araujo, L. O.; Zaioncz, S.; Floriano, J. B.; Macedo, A. G.; Araujo, C. M.; Marchiori, C. F. N.; Rodrigues, P. C. Assessing the Donor − Acceptor Nature and the Electrochemical Stability of a Fluorene − Diketopyrrolopyrrole − Thiophene-Based Copolymer. *Appl. Polym. Mater.* **2021**, *3*, 4223−4233.
(31) Corey, E. J.; Fuchs, P. L. A Synthetic Method for Formil -> Ethynyl Conversion. *Tetrahedron Lett.* **1972**, *13*, 3769−3772.
(32) Xu, W.; Hu, Q.; Bai, S.; Bao, C.; Miao, Y.; Yuan, Z.; Borzda, T.; Barker, A. J.; Tyukalova, E.; Hu, Z.; Kawecki, M.; Wang, H.; Yan, Z.; Liu, X.; Shi, X.; Uvdal, K.; Fahlman, M.; Zhang, W.; Duchamp, M.; Liu, J. M.; Petrozza, A.; Wang, J.; Liu, L. M.; Huang, W.; Gao, F. Rational Molecular Passivation for High-Performance Perovskite Light-Emitting Diodes. *Nat. Photonics* **2019**, *13* (6), 418−424.
(33) Wang, L.; Zhang, Z.; Wang, B.; Zhang, J. Fabrication of Perovskite Uniform Film in Air via Introduction of Aniline Cations. *ChemistrySelect* **2018**, *3* (24), 7023−7029.
(34) Chowdhury, T. H.; Kaneko, R.; Kaneko, T.; Sodeyama, K.; Lee, J.-J.; Islam, A. Electronic Defect Passivation of FASnI3 Films by Simultaneous Hydrogen-Bonding and Chlorine Co-Ordination for Highly Efficient and Stable Perovskite Solar Cells. *Chem. Eng. J.* **2022**, *431*, 133745.
(35) Xiong, S.; Song, J.; Yang, J.; Xu, J.; Zhang, M.; Ma, R.; Li, D.; Liu, X.; Liu, F.; Duan, C.; Fahlman, M.; Bao, Q. Defect-Passivation Using Organic Dyes for Enhanced Efficiency and Stability of Perovskite Solar Cells. *Sol. RRL* **2020**, *4* (5), 1900529.
(36) Akin, S.; Dong, B.; Pfeifer, L.; Liu, Y.; Graetzel, M.; Hagfeldt, A. Organic Ammonium Halide Modulators as Effective Strategy for Enhanced Perovskite Photovoltaic Performance. *Adv. Sci.* **2021**, *8* (10), 2004593.
(37) Sutanto, A. A.; Caprioglio, P.; Drigo, N.; Hofstetter, Y. J.; Garcia-Benito, I.; Queloz, V. I. E.; Neher, D.; Nazeeruddin, M. K.; Stolterfoht, M.; Vaynzof, Y.; Grancini, G. 2D/3D Perovskite Engineering Eliminates Interfacial Recombination Losses in Hybrid Perovskite Solar Cells. *Chem.* **2021**, *7* (7), 1903−1916.
(38) Koh, T. M.; Shanmugam, V.; Guo, X.; Lim, S. S.; Filonik, O.; Herzig, E. M.; Müller-Buschbaum, P.; Swamy, V.; Chien, S. T.; Mhaisalkar, S. G.; Mathews, N. Enhancing Moisture Tolerance in Efficient Hybrid 3D/2D Perovskite Photovoltaics. *J. Mater. Chem. A* **2018**, *6* (5), 2122−2128.
(39) Aristidou, N.; Eames, C.; Sanchez-Molina, I.; Bu, X.; Kosco, J.; Islam, M. S.; Haque, S. A. Fast Oxygen Diffusion and Iodide Defects Mediate Oxygen-Induced Degradation of Perovskite Solar Cells. *Nat. Commun.* **2017**, *8*, 1−10.
(40) Mosconi, E.; Azpiroz, J. M.; De Angelis, F. Ab Initio Molecular Dynamics Simulations of Methylammonium Lead Iodide Perovskite Degradation by Water. *Chem. Mater.* **2015**, *27* (13), 4885−4892.
(41) Li, Z.; Ji, J.; Zhang, C.; Hou, Q.; Jin, P. First-Principles Study on the Oxygen-Light-Induced Iodide Vacancy Formation in FASnI3Perovskite. *J. Phys. Chem. C* **2020**, *124* (26), 14147−14157.
(42) Bi, D.; Yi, C.; Luo, J.; Décoppet, J. D.; Zhang, F.; Zakeeruddin, S. M.; Li, X.; Hagfeldt, A.; Grätzel, M. Polymer-Templated Nucleation and Crystal Growth of Perovskite Films for Solar Cells with Efficiency Greater than 21%. *Nat. Energy* **2016**, *1* (10), 1−5.
(43) Li, N.; Cheng, C.; Wei, H.; Liu, H.; Li, X.; Li, W.; Wang, L. Enhanced Efficiency and Stability of Inverted Perovskite Solar Cells by Interfacial Engineering with Alkyl Bisphosphonic Molecules. *RSC Adv.* **2017**, *7* (67), 42105−42112.
(44) Gong, H.; Song, Q.; Ji, C.; Zhang, H.; Liang, C.; Sun, F.; Zhang, C.; Yang, A.; Li, D.; Jing, X.; You, F.; He, Z. Molecular Interactions and Functionalities of an Organic Additive in a Perovskite Semiconducting Device: A Case Study towards High Performance Solar Cells. *J. Mater. Chem. A* **2022**, *10* (6), 2876−2887.
(45) Fu, S.; Li, X.; Wan, L.; Wu, Y.; Zhang, W.; Wang, Y.; Bao, Q.; Fang, J. Efficient Passivation with Lead Pyridine-2-Carboxylic for High-Performance and Stable Perovskite Solar Cells. *Adv. Energy Mater.* **2019**, *9* (35), 1901852.
(46) Yang, S.; Dai, J.; Yu, Z.; Shao, Y.; Zhou, Y.; Xiao, X.; Zeng, X. C.; Huang, J. Tailoring Passivation Molecular Structures for Extremely Small Open-Circuit Voltage Loss in Perovskite Solar Cells. *J. Am. Chem. Soc.* **2019**, *141* (14), 5781−5787.
(47) Liang, L.; Luo, H.; Hu, J.; Li, H.; Gao, P. Efficient Perovskite Solar Cells by Reducing Interface-Mediated Recombination: A Bulky Amine Approach. *Adv. Energy Mater.* **2020**, *10*, 2000197.
(48) Wang, S.-Y.; Chen, C.-P.; Chung, C.-L.; Hsu, C.-W.; Hsu, H.-L.; Wu, T.-H.; Zhuang, J.-Y.; Chang, C.-J.; Chen, H. M.; Chang, Y. J. Defect Passivation by Amide-Based Hole-Transporting Interfacial Layer Enhanced Perovskite Grain Growth for Efficient p−i−n Perovskite Solar Cells. *ACS Appl. Mater. Interfaces* **2019**, *11* (43), 40050−40061.
(49) Chen, P.; Bai, Y.; Wang, S.; Lyu, M.; Yun, J. H.; Wang, L. In Situ Growth of 2D Perovskite Capping Layer for Stable and Efficient Perovskite Solar Cells. *Adv. Funct. Mater.* **2018**, *28* (17), 1706923.
(50) Hsiao, K.-C.; Jao, M.-H.; Li, B.-T.; Lin, T.-H.; Liao, S. H.-C.; Wu, M.-C.; Su, W.-F. Enhancing Efficiency and Stability of Hot Casting p−i−n Perovskite Solar Cell via Dipolar Ion Passivation. *ACS Appl. Energy Mater.* **2019**, *2* (7), 4821−4832.
(51) Liu, X.; Webb, T.; Dai, L.; Ji, K.; Smith, J. A.; Kilbride, R. C.; Yavari, M.; Bi, J.; Ren, A.; Huang, Y.et al. Influence of Halide Choice on Formation of Low-Dimensional Perovskite Interlayer in Efficient Perovskite Solar Cells. *Energy Environ. Mater.* **2022**, DOI: 10.1002/eem2.12321.
(52) Lanzetta, L.; Aristidou, N.; Haque, S. A. Stability of Lead and Tin Halide Perovskites: The Link between Defects and Degradation. *J. Phys. Chem. Lett.* **2020**, *11* (2), 574−585.
(53) Cui, Z.; Wang, M.; Lischka, H.; Kertesz, M. Unexpected Charge Effects Strengthen π−Stacking Pancake Bonding. *JACS Au* **2021**, *1* (10), 1647−1655.

https://doi.org/10.1021/jacsau.2c00151
JACS Au 2022, 2, 1306−1312